BioLegend®

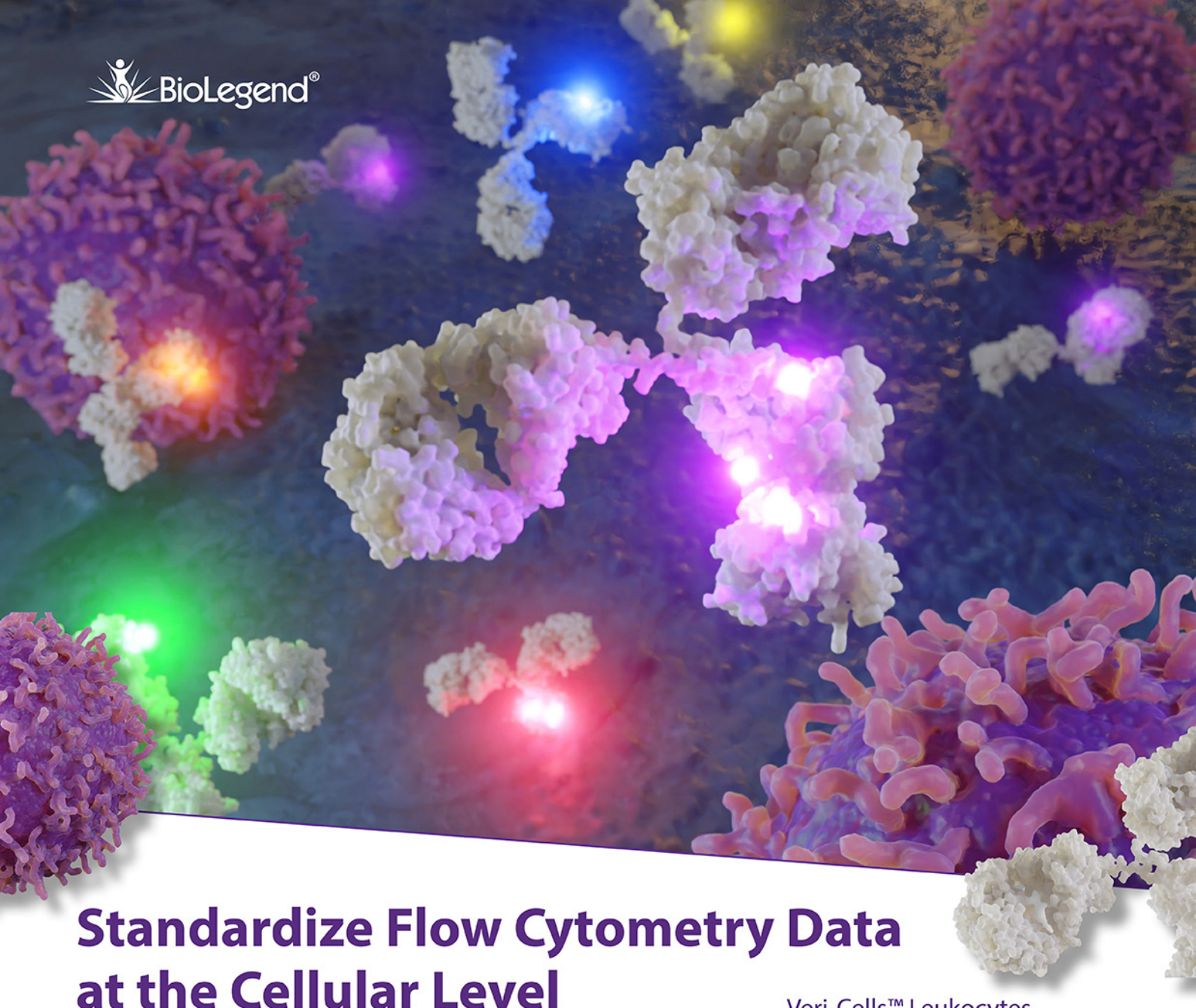

Standardize Flow Cytometry Data at the Cellular Level

Having the right controls for long-term studies is vital for flow cytometry experiments. To help researchers with this, we offer Veri-Cells™– lyophilized human control cells. These reagents have exceptional long-term stability, offer scatter profiles similar to fresh samples, and have been tested for 160+ markers. This allows researchers to monitor instrument performance and compare flow cytometry results in multicenter or longitudinal studies. Utilize them as controls for immunophenotyping, cellular activation, or mass cytometry experiments.

Discover the BioLegend difference with Veri-Cells™ for:

- Leukocytes
- PBMCs
- Cytokines
- Activation Markers
- Heavy Metals for CyTOF®

Veri-Cells™ Leukocytes

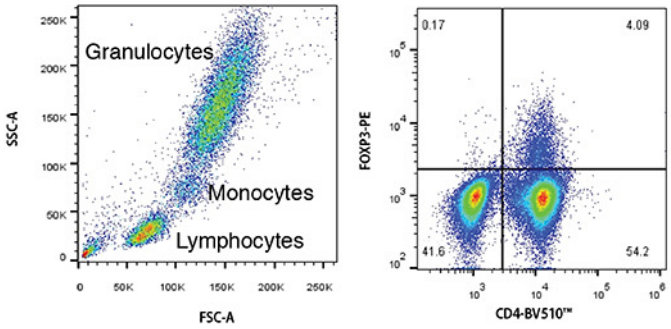

Veri-Cells™ Leukocytes were reconstituted and stained with indicated antibodies. The left plot displays the scatter profile, while the right plot demonstrates staining of surface CD4 and intranuclear FOXP3.

Learn more at: biolegend.com/veri-cells ▸

World-Class Quality | Superior Customer Support | Outstanding Value

BioLegend products are manufactured in an ISO 13485:2016-certified facility to ensure the highest quality standards.

biolegend.com

Received: 19 October 2021 | Revised: 19 April 2022 | Accepted: 22 April 2022

DOI: 10.1002/cyto.a.24562

BRIEF REPORT

MIFlowCyt

ISAC INTERNATIONAL SOCIETY FOR ADVANCEMENT OF CYTOMETRY

CYTOMETRY Journal of Quantitative Cell Science PART A

Redistribution of CD8+ T cell subsets in metastatic renal cell carcinoma patients treated with anti-PD-1 therapy

Sara De Biasi[1] | Annalisa Guida[2,3] | Domenico Lo Tartaro[1,4] | Martina Fanelli[1,3] | Roberta Depenni[3] | Massimo Dominici[1,3] | Greg Finak[5] | Camillo Porta[6] | Annamaria Paolini[1,4] | Rebecca Borella[1,4] | Carlo Bertoldi[7] | Andrea Cossarizza[1,8] | Roberto Sabbatini[3] | Lara Gibellini[1]

[1]Department of Medical and Surgical Sciences for Children & Adults, University of Modena and Reggio Emilia, Emilia-Romagna

[2]Azienda Ospedaliera Santa Maria, Terni, Italy

[3]Department of Oncology, University of Modena & Reggio Emilia, Modena, Italy

[4]Clinical and Experimental Medicine PhD Program, University of Modena and Reggio Emilia, Modena, Italy

[5]Fred Hutchinson Cancer Research Center, Seattle, USA

[6]Chair of Oncology, University of Bari, Bari, Italy

[7]Department of Surgery, Medicine, Dentistry and Morphological Sciences, University of Modena and Reggio Emilia, Italy

[8]National Institute for Cardiovascular Research, Bologna

Correspondence
Lara Gibellini and Andrea Cossarizza, Department of Medical and Surgical Sciences for Children & Adults, University of Modena and Reggio Emilia, Emilia-Romagna, Italy.
Email: lara.gibellini@unimore.it and andrea.cossarizza@unimore.it

Funding information
This work was funded by Fondazione Cassa di Risparmio di Modena to GP (2017); by Fondo di Ateneo per la Ricerca (FAR) 2017 to AC; by unrestricted grants to AC from: Sanfelice 1873 Banca Popolare (San Felice sul Panaro,

Abstract

Renal-cell carcinoma (RCC) is responsible for the majority of tumors arising from the kidney parenchyma. Although a progressive improvement in median overall survival has been observed after the introduction of anti-PD-1 therapy, many patients do not benefit from this treatment. Therefore, we have investigated T cell dynamics to find immune modification induced by anti-PD-1 therapy. Here, we show that, after therapy, RCC patients (5 responders and 14 nonresponders) are characterized by a redistribution of different subsets across the memory T cell compartment.

KEYWORDS
anti-PD-1 therapy, mRCC, single-cells technologies, T cells, unsupervised cluster analysis

Sara De Biasi, Annalisa Guida, and Domenico Lo Tartaro contributed equally to this work.

Roberto Sabbatini and Lara Gibellini should be considered co-senior authors.

Modena, Italy), Rotary CLUB Distretto 2072 (Modena, Modena L.A. Muratori, Carpi, Sassuolo, Ca-stelvetro di Modena, Italy).; Rotary CLUB Distretto 2072; Sanfelice 1873 Banca Popolare; Fondo di Ateneo per la Ricerca; Fondazione Cassa di Risparmio di Modena

1 | INTRODUCTION

Renal-cell carcinoma (RCC) accounts for about 5% and 3% of all malignancies in men and women respectively, and at diagnosis almost 15% of these tumors shows metastasis [1]. Metastatic renal-cell carcinoma (mRCC) has a poor prognosis, although a progressive improvement in median overall survival (OS) has been observed after the introduction of targeted therapy [2]. Since 2015, the management of mRCC was revolutionized by the introduction of immune checkpoints inhibitors (ICI), that is, anti-cytotoxic T-lymphocyte associated protein 4 (CTLA-4, or CD152), anti-programmed cell death-1 (PD-1, or CD279), and anti-programmed death-ligand 1 (PD-L1, or CD274) monoclonal antibodies [2–4]. CTLA-4 and PD-1/PD-L1 are key elements in immune tolerance and main regulators of T-cell-mediated antitumor immune response, respectively [5]. During the past few years, significant increase in life expectancy, together with lasting responses, allowed the approval of different combinations of drugs for treating mRCC patients, in both first- and second-line settings, that are: (i) nivolumab (anti-PD-1), administered either alone or in combination with ipilimumab (anti-CTLA-4), or with the multikinase inhibitor cabozantinib; (ii) of pembrolizumab (anti-PD-1), given in combination with axitinib or lenvatinib; and (iii) avelumab (anti-PD-L1), used in combination with axitinib [3,6–8]. ICI have dramatically modified the prognosis of several patients with mRCC, but unfortunately only a subset of patients benefits from these treatments [9]. The reasons at the basis of the lack of benefit are still largely unknown.

Basic and clinical research is focusing on the immunological effects of checkpoint inhibitors to identify predictors or early indicators of response. Monitoring of peripheral immune cells is very attractive, given the ease of blood sample collection and the possibility to follow different parameters over time [10]. Indeed, a large body of studies describes changes in peripheral markers after the treatment with ICI in different types of cancers [11].

Even if compelling efforts have been made to characterize the mode of action of immunotherapies and identify markers that could predict a clinical response in patients, currently there are scanty data regarding changes among peripheral blood mononuclear cells (PBMC) in mRCC. Recently, advanced clear-cell RCC was dissected via spatially segregated multimodal single-cell genomics [12]. It was found that great heterogeneity was present within and between patients, with enrichment of CD8A+ tissue-resident T cells in a patient responsive to immune checkpoint blockade, and tumor-associated macrophages in a resistant patient [12].

Here, we used high-parameter flow cytometry to address the impact of PD-1 inhibition on circulating immune cells in patients with mRCC.

2 | MATERIALS AND METHODS

2.1 | Patients

The study was conducted on 19 patients with metastatic renal carcinoma treated with standard-of-care nivolumab at the Division of Oncology—Azienda Ospedaliero Universitaria di Modena and Reggio Emilia. According to RECIST, 5 patients were classified as responders (R) and 14 as nonresponders (NR). The clinicopathologic characteristics of patients are reported in Table 1. According to the international metastatic RCC database consortium (IMDC) 60% of R patients had a good prognosis and 64.3% of NR patients had an intermediate prognosis.

The mean age of the total cohort was 69 years (range 55–81). Eighty-four percent of patients showed lung metastasis. All patients had previously received other therapies: 52.7% received one previous therapy, 31.5% received two previous therapies, and 15.8% received three previous therapies.

2.2 | Blood collection

Blood samples (up to 30 ml) were obtained after informed consent through the Azienda Ospedaliero Universitaria di Modena and Reggio Emilia. Approval of study protocols was obtained by the local ethical committee (Protocol AOU 195/2016). Blood was obtained before therapy (hereafter indicated as T0), and after the first, second, and third cycle of therapy (hereafter indicated as T1, T2, and T3, respectively). All patients were treated with the immune checkpoint inhibitor Nivolumab, an anti-PD1 drug, every 14 days. PBMC were isolated according to standard procedures and stored in liquid nitrogen until use [13].

2.3 | Polychromatic flow cytometry

A 28 parameter/26-color flow cytometry panel was optimized to broadly characterizes T cell differentiation and activation along with markers that are target or are involved in immunotherapy response (CD3, CD4, CD8, CD45RA, CD197, CD28, CD27, CD127, CD95, CD98, CD71, CD25, HLA-DR, CD38, CD39, CXCR6, CCR4, KI67, T-bet, granulysin, PD-1, BTLA, CD57, CD244, and ICOS). Moreover,

TABLE 1 Demographic and clinical characteristics of patients

Variable	Responders ($n = 5$)	Nonresponders ($n = 14$)
Demographic characteristics		
Age, mean year (range)	71 (58–82)	70.9 (56–81)
Male sex, *N* (%)	4 (80)	11 (78.5)
BMI Kg/mq, mean (range)	26.4 (20.7–31.8)	23.5 (18.3–28.5)
Clinical characteristics		
Years from diagnosis, mean (range)	12 (4–22)	12.1 (4–30)
Fuhrman grade of renal-cell carcinoma		
1 or 2, *N* (%)	1 (20.0)	6 (42.8)
3 or 4, *N* (%)	3 (60.0)	5 (35.7)
Unknown, *N* (%)	1 (20.0)	3 (21.5)
Tumor stage		
T1, *N* (%)	1 (20.0)	5 (35.7)
T2, *N* (%)	3 (60.0)	3 (21.5)
T3, *N* (%)	1 (20.0)	4 (28.5)
Tx, *N* (%)	0 (0)	2 (14.3)
Median number of metastatic sites (range)	2.7 (2–5)	2.7 (1–6)
Location of metastasis		
Lung, *N* (%)	5 (100.0)	11 (78.6)
Liver, *N* (%)	0 (0)	2 (14.3)
Lymph nodes, *N* (%)	5 (100.0)	5 (35.7)
Pancreas, *N* (%)	1 (20.0)	3 (21.4)
IMDC prognosis		
Good	3 (60.0)	1 (7.1)
Intermediate	2 (40.0)	9 (64.3)
Poor	0 (0)	4 (28.6)
Blood parameters		
Basal white blood cells, *N*/μl	6351	6483
Basal neutrophils, mean *N*/μl	4259	4439
Basal lymphocytes, mean *N*/μl	1580	1579
Basal CRP, mean mg/L	4.4	4.7
Previous therapy		
One previous therapy, *N* (%)	3 (60.0)	7 (50.0)
Two previous therapies, *N* (%)	0 (0)	6 (42.8)
Three or more previous therapies, *N* (%)	2 (40.0)	1 (7.2)

the panel was optimized to identify the expression of PD-1 in T cells isolated from patients treated with anti-PD-1 (either nivolumab or pembrolizumab) as anti-IgG4 was used to recognize the anti-PD-1 bound to PD-1 [14]. Two antibodies cocktail were prepared for staining: one that contains anti-PD1 (clone EH12.1) used for the detection of the expression of PD-1 at T0, that is, before therapy initiation; the other antibody cocktail with anti-IgG4 for the detection of cell surface PD-1 bind by Nivolumab. This latter antibody cocktail has been used for all the time points except T0 and does not contain anti-PD1 mAb.

Briefly, cryopreserved samples were thawed in R10 medium, that is, RPMI supplemented with 10% fetal bovine serum (FBS), 100 U/ml penicillin, 100 μg/ml streptavidin, 2 mM L-glutamine, 20 mM HEPES (ThermoFisher, Eugene, OR) and 20 μg/ml DNase I from bovine pancreas (Sigma-Aldrich, St. Louis, MO) [13]. After washing with phosphate buffer saline (PBS), cells were stained immediately with the Zombie Aqua Fixable Viability kit (BioLegend, San Diego, CA) for 15 min at room temperature. Then, cells were washed and stained with the combination of monoclonal antibodies (mAbs) purchased from either Becton Dickinson Biosciences (BD, San José, CA), BioLegend, or eBioscience/ThermoFisher (Eugene, OR), as listed in Table S1, that reports also the fluorochromes bound to the different monoclonal mAbs, that had been previously titrated to define the optimal concentration. Chemokine receptors were stained for 20 min at 37°C. Intracellular detection of KI-67, granulysin and T-bet was performed following fixation of cells with the FoxP3 transcription factor staining buffer set (eBioscience/ThermoFisher) according to manufacturer's instructions and by incubating with specific mAbs for 30 min at 4°C. Samples were acquired on a FACS Symphony A5 flow cytometer (BD Biosciences) equipped with five lasers (UV, 350 nm; violet, 405 nm; blue, 488; yellow/green, 561 nm; red, 640 nm) and capable to detect 30 parameters. Flow cytometry data were compensated in FlowJo by using single stained controls (BD Compbeads incubated with fluorochrome-conjugated antibodies) [13]. Gating strategy is shown in Figure S1A, and representative dot plots for different markers are shown in Figure S1B,C. All the antibodies used in the panel are reported in Table S1.

2.4 | High-dimensional flow cytometry data analysis

Flow cytometry standard (FCS) 3.0 files were imported into FlowJo software version 10, compensated and biexponentially transformed. Then debris, aggregates, doublets, and dead cells were excluded. Overlaying fluorescence histograms of all samples were used to identify differences in staining, background fluorescence and transformation (using Flowjo). The following markers HLA-DR, ICOS, and Ki67 were excluded from the analysis due to batch error across multiple batches. We imported basic FlowJo workspaces into R to create a gating set by using flowWorkspace (v4.0.6). For CD8+ T cell analysis, "Live CD8" T cells gate was selected as startingNode and manually set channel bounds according to the FlowJo marker's distribution. FAUST makes minimal assumptions about the distribution of markers, according to this it detects the different sub-population in a data-driven fashion. To perform this, FAUST generates an annotation forest for each experimental unit (each sample). Then, FAUST calculates a standardized set of boundary thresholds and the separation-score "depth score" for each marker by sample. The depth score quantifies how consistently a marker separates into subpopulations in the

annotation forest. Next, after the selection of a subset of high-scoring markers in the panel, FAUST use the sample-specific marker boundary to perform the clustering (annotation). In our analysis, the following markers showed the highest "depth score" and were selected for clustering: CD45RA, CD57, TBET, CD28, CD127, CD38, CCR7, GRANULYSIN, CD95, CXCR6, and PD1 (Indicated as PD1_IGG4). For CD4+ T cell analysis, "Live CD4" T cells gate was selected as startingNode and manually set channel bounds according to the FlowJo marker's distribution. The following markers showed the highest "depth score" and were selected for clustering: CD45RA, CD57, TBET, CD28, CD27, CD127, CD38, CCR7, GRANULYSIN, CD95, CD39, PD-1 (Indicated as PD1_IGG4). Analysis was performed without downsampling. "FAUST" (v 0.5.1) was run by setting tuning parameters "samplename" for the experimentalUnit and "1" for nameOccuranceNum. The depthScoreThreshold and selectionQuantile were selected analyzing the depth score line plots. The final countMatrix was filtered choosing the clusters that were at least 50% of samples with at least 200 cells for each phenotype. The nonlinear dimensional reduction was performed using Uniform Manifold Approximation and Projection (UMAP) algorithm (uwot v.0.1.8) through makeAnnotationEmbedding function. Finally, all data were graphed with ggplot2 (v. 3.3.2) using a custom script. UMAP representation of the CD8+ T cell landscape (all patients and all timepoints are included) are reported in Figure S2. FAUST separation-score "depth score" for each marker by sample for CD8+ and CD4+ T cells, Ridgeplots for CD4 and CD8 T cells, UMAP projections of expression of the indicated proteins for CD8+ and CD4+ T cells are reported in Figures S3B and S4B. The percentage of CD4+ and CD8+ T clusters obtained by FAUST analysis are provided as sourcedata file (sourcedata_RCC).

2.5 | In vitro cytokine production

Thawed PBMC were rested for 4 h at 37°C and then in vitro stimulated with anti-CD3/CD28 (1 μg/ml) (Miltenyi, Bergisch Gladbach, Germany) and suboptimal concentration of IL-2 (10 ng/ml) (Miltenyi). For each sample, at least 2 million cells were left unstimulated as negative control and 2 million cells were stimulated. All samples were incubated with a protein transport inhibitor containing brefeldin A (Golgi Plug, BD). [15]

A 12 parameter/10-color flow cytometer panel was optimized to identify different subpopulations of T cells producing TNF, IFN-γ, and IL-2 that were detected after 16 h of incubation (Table S2). For the quantification of intracellular cytokines, cells were fixed with BD Cytofix/Cytoperm Fixation/Permeabilization Solution kit (BD Biosciences) according to the manufacturer's instructions. Samples were acquired on an Attune NxT acoustic flow cytometer (ThermoFisher) equipped with four lasers (violet, 405 nm; blue, 488; yellow/green, 561 nm; red, 640 nm) and capable to detect 14 parameters. Flow cytometry data were compensated in FlowJo by using single stained controls as above. Gating strategy is shown in Figure S5.

2.6 | Statistical analysis

Statistical analyses were performed using GraphPad Prism version 8 (GraphPad Software Inc., La Jolla), unless specified otherwise. To compare distributions of manually gated subsets significance was determined by Kruskal-Wallis test, unless otherwise specified in the figure legends. Simplified Presentation of Incredibly Complex Evaluation (SPICE) software (version 6, kindly provided by Dr. Mario Roederer, Vaccine Research Center, NIAID, NIH, Bethesda, MD) was used to analyze flow cytometry data on T cell polyfunctionality [16]. The two-way analysis of variance (ANOVA) with Bonferroni correction was used to test each sub-population for differential abundance during the timepoint therapy in R versus NR.

3 | RESULTS

3.1 | mRCC patients displayed a decrease of TSCM and increase of TEM cell percentages after therapy

Changes in CD8+ T cell dynamics have been investigated by using 28-parameters flow cytometry and analyzed by Full Annotation Using Shape-constrained Trees (FAUST), a novel non-parametric method for unbiased discovery of cell population in single-cell flow cytometry [17]. Clustering was performed using differentiation and functional markers such as CD45RA, CD57, TBET, CD28, CD127, CD38, CCR7, GRANULYSIN, CD95, PD1, and CXCR6.

Sixty-one cell clusters were identified that represent the entire differentiation spectrum of CD8+ T cells. In particular, we identified: 4 clusters of naïve (N) T cell, 3 clusters of TSCM, 2 cluster of central memory T cells (CM), 12 clusters of transitional memory (TM) cells, 13 clusters of effector memory (EM) T cells and 27 clusters of terminally differentiated effector memory (EMRA) T cells (File S1 and Figure S2).

First, statistical analyses were performed dividing patients on the basis of the response to therapy. Responder (R, $n = 5$) and non-responder (NR, $n = 14$) patients were compared for all the clusters identified, but due to low number of patients responding to therapy, we found similar percentages of clusters in R and NR (Figure S6) at all timepoints. However, considering all patients treated with anti-PD1 ($n = 19$), we show that therapy was able to induce a redistribution of the different subpopulations of CD8+ T cells (Figure 1 and Figure S7). Naïve compartment, identified as the cluster of cells that were CD45RA+CD57-TBET-CCR7+CD28+CD127+CD38-GRANULYSIN-CXCR6-CD95-PD1_IgG4-, decreases after the third cycle of therapy. It is to note that, even before therapy, in these patients the percentage of naïve T cell was very low. This could be congruent with the relatively advanced age of mRCC patients (range 55–81 years) and with the fact that their immune system could have been challenged by 10 years of disease (see Table 1 for demographic and clinical characteristics of the patients included in the study). One of the underpinning of T cell immune decline and cancer is that in the elderly there is a reduction in the proportion of naïve T cells and in their diversity,

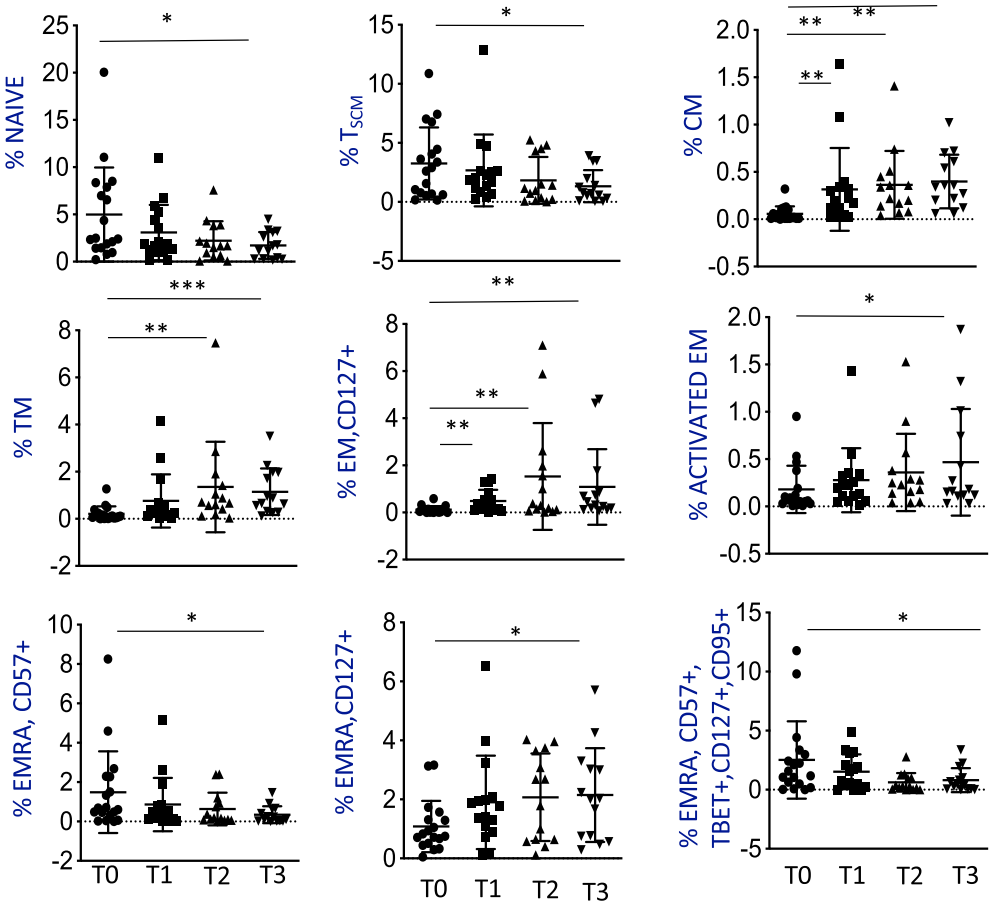

FIGURE 1 Percentages of different subpopulations of CD8+ T cells identified by FAUST. Data represent individual values, mean (centre bar) ± *SD* (upper and lower bars). N, naïve; TSCM, stem cell memory T cells; CM, central memory; TM, transitional memory; EM, effector memory; EMRA, terminally differentiated effector memory. T0, before therapy; T1, after 1 cycle of therapy; T2, after 2 cycles of therapy; T3, after three cycles of therapy. All the populations have been defined in the results section according to their marker expression. The following markers have been used to define T cell subpopulations: CD45RA, CD57, TBET, CCR7, CD28, CD127, CD38, GRANULYSIN, CXCR6, CD95, PD1/IgG4. One-way ANOVA was applied, *p*-value: * < 0.05; ** < 0.001 [Color figure can be viewed at wileyonlinelibrary.com]

leading to a dominant memory T cell pool [18]. After therapy, TSCM subset, identified as CD45RA+CD57-TBET-CD28+CD127+-CD38-CCR7+ GRANULYSIN- CXCR6-CD95+PD1_IgG4-, decreased by 2.5-fold passing from a mean value of 3.26%, measured before therapy, to 1.32%, measured after the third cycle of therapy (Figure 1). Whereas TSCM cells are considered the most pluripotent, CM cells are capable of give origin to EM subsets and to a cluster of CM T cells (CD45RA-CD57-TBET-CCR7+CD28+CD127+-CD38-GRANULYSIN-CXCR6-CD95-PD1_IgG4-) that increased after the first, the second and the third cycle of therapy (Figure 1).

The effector memory compartments increased after therapy. A total of 2 EM clusters were affected by therapy initiation (Figure 1). Discrimination between distinct stages of human CD8+ T-cell differentiation has often relied upon the cell surface expression of CD27 and CD28, costimulatory molecules of distinctive functions. Interaction of CD28 with CD80 and CD86 on antigen-presenting cells amplifies T-cell proliferation and activation through a series of direct effects. T cell differentiation has been proposed wherein CD27+ CD28+ CD45RA+ naive cells progress through a CD27+ CD28+ CD45RA- early antigen-experienced phenotype to a CD27+ CD28- CD45RA-/+ intermediate phenotype and finally to a CD27- CD28- CD45RA+/- late antigen-experienced phenotype that parallels an increased cytotoxic potential and reduced ability to proliferate [19]. Here, a TM subset, identified as CD45RA-CD57-TBET-CCR7-CD28+CD127+CD38-GRANULYSIN-CXCR6-CD95-PD1_IgG4-, increased from a mean value of 0.21%, measured before therapy, to 1.15%, measured after the third cycle of therapy (Figure 1).

The expression of CD127, the alpha chain of IL-7 receptor, on cell membrane is very important for T cell homeostasis and is a useful marker for measuring long-living memory T cells. Most importantly, its expression allows the distinction between memory and effector T cells early after in vivo priming. EM subsets expressing or not CD127 (CD45RA-CD57-TBET-CCR7-CD28-CD127-/+CD38-GRANULYSIN-CXCR6-CD95-PD1_IgG4-), increased after the third cycle of therapy. In addition, CD45RA-CD57-TBET-CCR7-CD28+CD127+CD38+-GRANULYSIN-CXCR6-CD95+PD1_IgG4- cells, identified as activated EM, increased after the third cycle of therapy (Figure 1).

Previous studies have demonstrated that both T-bet and Eomes are involved in the generation of effector and central memory CD8 T cells. T-bet is an essential regulator of effector differentiation and function in multiple different immune lineages. Inflammatory cytokines induce T-bet expression, which in turn regulates distinct differentiation outcomes. For example, T-bet can act as a fulcrum between Th1 and Tfh cell differentiation, pathogenic and nonpathogenic Th17 cells, and CD8 effector and memory T cells. T-bet induces CXCR3 expression on multiple different lymphocytes promoting an effective immune response by allowing the homing of different cells in the

inflamed tissue [20]. EM clusters expressing TBET identified as CD45RA-CD57-TBET+CCR7-CD28-CD127+/-CD38-GRANULYSIN-CXCR6-CD95-PD1_IgG4-, increased after therapy, too (Figure 1).

CD45RA+CCR7- EMRA cells are found more frequently in the CD8+ compartment, are generally negative for CD27 and CD28, and display the shortest telomeres among T cells. EMRA cells express markers of senescence, including KLRG-1, CD57, and phosphorylation of histone H2AX, and have low proliferative and functional capacity indicating terminal differentiation [21]. Moreover, CD8+EMRA T cells display a senescence-associated secretory phenotype regulated by p38 MAPK [20]. Seven EMRA clusters were affected by anti-PD1 therapy. A cluster of EMRA expressing or not CD127, identified as CD45RA+CD57-TBET-CCR7-CD28-CD127-CD38-GRANULYSIN-CXCR6-CD95-PD1_IgG4-, increased after the third cycle of therapy as well as a cluster of EMRA cells expressing CD28 (CD45RA+CD57-TBET-CCR7-CD28+CD127-CD38-GRANULYSIN-CXCR6-CD95-PD1_IgG4-) and one expressing TBET (CD45RA+CD57-TBET+-CCR7-CD28-CD127+CD38-GRANULYSIN-CXCR6-CD95-PD1_IgG4-). On the contrary, a terminally differentiated cluster of EMRA expressing CD57, TBET and CD95 (CD45RA+CD57+TBET+CCR7-CD28-CD127+CD38-GRANULYSIN-CXCR6-CD95+PD1_IgG4) decreased after therapy from (Figure 1).

Finally, CD4 T cell subset has been investigated. Two clusters out of 44 have been modulated during the therapy. These clusters identified activated CM cells (CD45RA-CD95-CD39-CD57-CCR7+CD28+-TBET-CD38+GRANULYSIN-CD127+CD27-PD1_IGG4-), which decrease during therapy ($p = 0.0263$) and naïve cells (CD45RA+CD95-CD39-CD57-CCR7+CD28+TBET-CD38-GRANULYSIN-CD127+CD27+PD1_IGG4-) whose percentage increase ($p = 0.0336$; Figure S8).

3.2 | Cytokine production is increased in more undifferentiated cells after therapy

To ascertain the capability of therapy to reactivate the pro-inflammatory function of CD8+ T cells, PBMC were in vitro stimulated by using anti-CD3 plus anti-CD28. Then, the percentages of CD8+ T cell subpopulations producing one or more cytokines, such as IFN-γ and TNF together with IL-2, were quantified.

Overall, similar percentages of CD8+ T cells producing different cytokines were found after therapy, but, looking at the different subpopulations of T cells, we noted that TSCM as well as CM producing IFN-γ and TNF increased after the second cycle of therapy. In terms of polyfunctionality, we found higher percentages of TSCM able to produce simultaneously TNF and IFN-γ. No differences were found in terms of cells producing IL-2. This suggests that the pools of more undifferentiated cells are able to exert pro-inflammatory activity after in vitro stimulation (Figure 2). No differences in terms percentages of cells producing IFN-γ and TNF after therapy were found among EM and EMRA (Figure S9) nor within CD4 T cell subsets (Figure S10).

4 | DISCUSSION

Despite the impressive clinical improvements achieved with immunotherapy in mRCC management, a large part of patients eventually fails to respond to this therapy, due to the onset of primary or secondary resistance. Clinical definition of tumor resistance to immunotherapy is clearly established, defining primary resistance as the clinical *scenario* where a cancer does not respond to an immunotherapy strategy, and secondary resistance as the clinical condition in which a cancer initially responded to immunotherapy, but after a period of time it relapsed and progressed [22]. Currently, a crucial unmet need is to early recognize primary refractory mRCC, and thus every attempt to clarify mechanism of resistance is necessary. The early identification of primary resistant patients represents a major challenge in mRCC management to optimize treatment strategies.

Our data suggest that anti-PD1 therapy induces a redistribution of peripheral CD8+ T cell subpopulations in mRCC patients. The most relevant difference involves the decrease of Naïve and TSCM pools and the increase of effector memory compartment, spanning from transitional memory cells to terminally differentiated effector memory elements. These results outline how in primary refractory patients an anti-PD1 treatment is active but not effective, resulting in early progression of disease with almost no clinical benefit.

During the last decade, the immune response mediated by T cells in cancer patients treated with ICI has been deeply investigated by analyzing both tumor-infiltrating lymphocytes [23–26] and circulating T cells [27–29]. It was found that distinct CD8+ T cell subsets are enriched after immune checkpoint blockade, both in the tumor and in peripheral blood. However, the mechanisms at the basis of these changes have not been identified. Recently, determinants of anti-PD-1 response and resistance in clear cell renal cell carcinoma has been largely investigated with single cell technologies revealing that nivolumab drives both maintenance and replacement of previously expanded T cell clones. However, only maintenance of these clones correlates with response supporting the idea that maintenance and boosting of a pre-existing response is a key element of anti-PD-1 mode of action [30].

Here we show a redistribution of circulating T cells after anti-PD1 therapy in with a reduction of the percentage of naïve T cells and with an increase of effector memory T cell compartment, likely suggesting that the naïve compartment is consumed after therapy giving origin to EM cells, showing the discrepancy between treatment activity and lack of response in primary refractory mRCC patients.

We are well aware that this study has several limitations. The first is represented by the relatively low number of patients enrolled in the study, the lack of absolute lymphocyte count and by their clinical characteristic, as all of them were treated with anti-PD1 in second or third line of therapy and most patients not

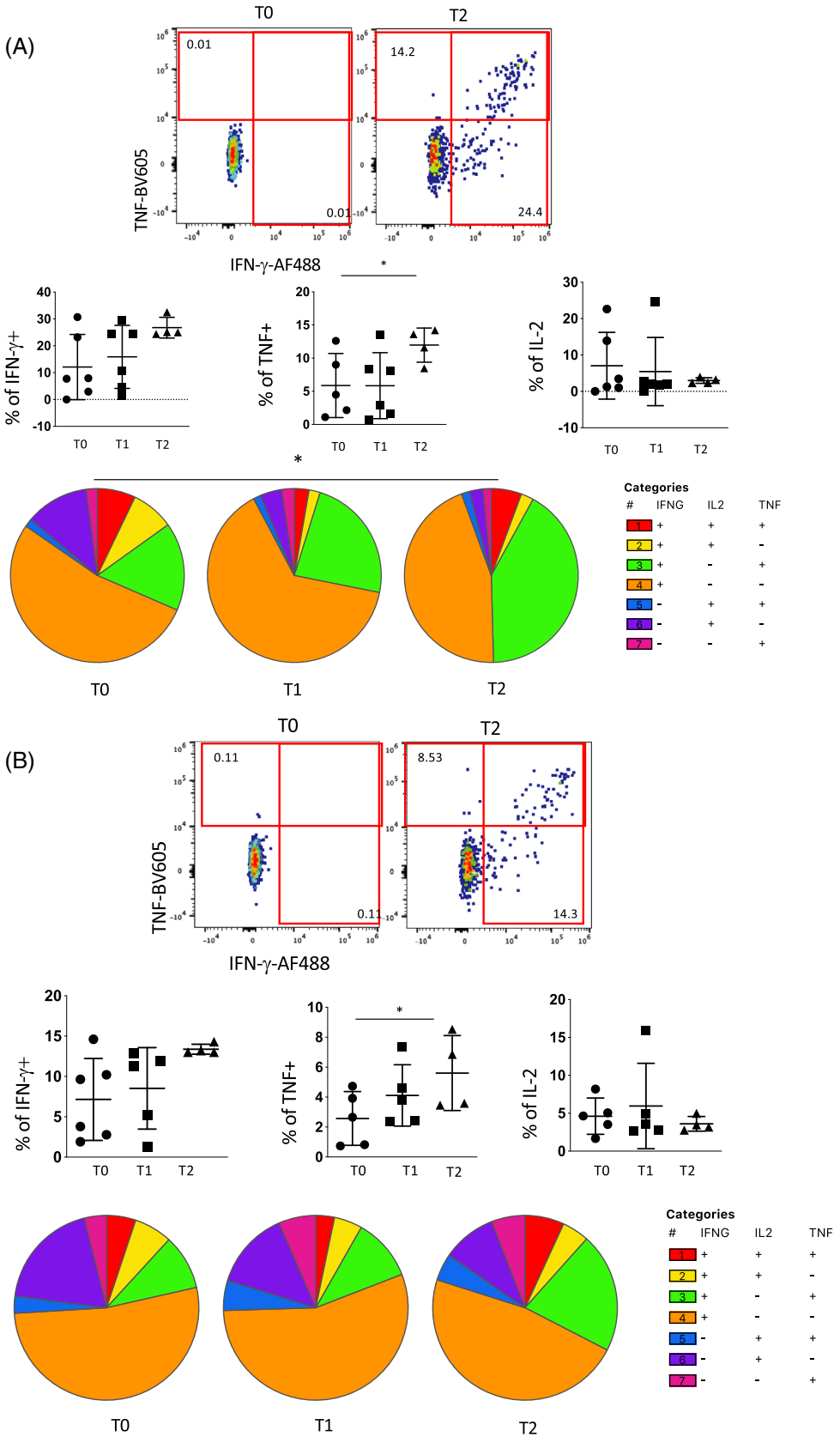

FIGURE 2 CD8+ T cell subpopulation cytokine production evaluated after in vitro stimulation. (A) Representative dot plots of TSCM producing TNF and IFN-γ after in vitro stimulation before (T0) and after two cycles of therapy (T2). Percentage of cells producing IFN-γ and TNF is also reported. Data represent individual values, mean (center bar) ± *SD* (upper and lower bars). Kruskal-Wallis one-way ANOVA was used for statistical analysis (upper row). Pie charts represent polyfunctional response of TSCM after in vitro stimulation before and after therapy. Permutation test has been used (lower row). RCC patients, $n = 6$. (B) Representative dot plots of TCM producing TNF and IFN-γ after in vitro stimulation before (T0) and after two cycles of therapy (T2). Percentage of cells producing IFN-γ and TNF is also reported. Data represent individual values, mean (center bar) ± *SD* (upper and lower bars). Kruskal-Wallis one-way ANOVA was used for statistical analysis (upper row). Pie charts represent polyfunctional response of TCM after in vitro stimulation before and after therapy. Permutation test has been used (lower row). RCC patients, $n = 6$ [Color figure can be viewed at wileyonlinelibrary.com]

responding to therapy. Second, due to ethical and clinical restraints, sampling of tumor biopsies from these patients was not possible. This limits the possibilities for intratumoral immunophenotyping and mechanistic investigations. Third, the amount of cells that we could obtain did not allow further functional investigation, and all the metabolic aspects of the cells of interest still await a detailed analysis.

AUTHOR CONTRIBUTIONS

Sara De Biasi: Conceptualization (equal); data curation (equal); writing – original draft (lead); writing – review and editing (lead). **Annalisa Guida:** Data curation (equal). **Domenico Lo Tartaro:** Formal analysis (lead); software (lead). **Martina Fanelli:** Data curation (supporting). **Roberta Depenni:** Investigation (supporting). **Massimo Dominici:** Investigation (supporting). **Greg Finak:** Methodology (supporting); software (supporting). **Camillo Porta:** Investigation (supporting). **Annamaria Paolini:** Methodology (supporting). **Rebecca Borella:** Methodology (supporting). **Carlo Bertoldi:** Methodology (supporting). **Andrea Cossarizza:** Conceptualization (lead); funding acquisition (lead); supervision (lead); writing – original draft (lead). **Roberto Sabbatini:** Data curation (lead); formal analysis (lead); investigation (lead). **Lara Gibellini:** Conceptualization (lead); supervision (supporting); validation (lead); writing – original draft (equal); writing – review and editing (equal).

ACKNOWLEDGMENTS

We thank Paola Paglia (ThermoFisher), Leonardo Beretta (Beckman Coulter), Enrico Lugli, Federica De Paoli and Federico Colombo (Humanitas Clinical and Research Center, Rozzano, Milan, Italy) for the precious technical advice and continuous support. Sara De Biasi and LG have been or are Marylou Ingram Scholar of the International Society for Advancement of Cytometry (ISAC) for the period 2012–2016, 2016–2020, and 2020–2024, respectively. We are grateful to all the patients who donated blood for this study. Open Access Funding provided by Universita degli Studi di Modena e Reggio Emilia within the CRUI-CARE Agreement.

ETHICS STATEMENT

The study was conducted according to the guidelines of the Declaration of Helsinki and approved by the Ethics Committee of "Area Vasta Emilia Nord" (Protocol AOU 195/2016).

FUNDING INFORMATION

This work was funded by Fondo di Ateneo per la Ricerca (FAR) 2017 to Andrea Cossarizza; by unrestricted grants to Andrea Cossarizza from: Sanfelice 1873 Banca Popolare (San Felice sul Panaro, Modena, Italy), Rotary CLUB Distretto 2072 (Modena, Modena L.A. Muratori, Carpi, Sassuolo, Castelvetro di Modena, Italy).

INFORMED CONSENT STATEMENT

Informed consent was obtained from all subjects involved in the study.

CONFLICT OF INTEREST

The authors declare no conflict of interest.

DATA AVAILABILITY STATEMENT

FCS files of all RCC patients at different timepoints are available in Flow Repository folder ID: FR-FCM-Z4LE.

ORCID

Sara De Biasi https://orcid.org/0000-0002-3217-9821
Greg Finak https://orcid.org/0000-0003-4341-9090
Andrea Cossarizza https://orcid.org/0000-0002-5381-1558

REFERENCES

1. Siegel RL, Miller KD, Jemal A. Cancer statistics, 2018. CA Cancer J Clin. 2018;68(1):7–30.
2. Saad AM, Gad MM, Al-Husseini MJ, Ruhban IA, Sonbol MB, Ho TH. Trends in renal-cell carcinoma incidence and mortality in the United States in the last 2 decades: a SEER-based study. Clin Genitourin Cancer. 2019;17(1):46–57 e45.
3. Motzer RJ, Escudier B, McDermott DF, George S, Hammers HJ, Srinivas S, et al. Nivolumab versus Everolimus in advanced renal-cell carcinoma. N Engl J Med. 2015;373(19):1803–13.
4. Motzer RJ, Tannir NM, McDermott DF, Aren Frontera O, Melichar B, Choueiri TK, et al. Nivolumab plus Ipilimumab versus Sunitinib in advanced renal-cell carcinoma. N Engl J Med. 2018;378(14):1277–90.
5. Robert C. A decade of immune-checkpoint inhibitors in cancer therapy. Nat Commun. 2020;11(1):3801.
6. Choueiri TK, Powles T, Burotto M, Escudier B, Bourlon MT, Zurawski B, et al. Nivolumab plus Cabozantinib versus Sunitinib for advanced renal-cell carcinoma. N Engl J Med. 2021;384(9):829–41.
7. Motzer R, Alekseev B, Rha SY, Porta C, Eto M, Powles T, et al. Lenvatinib plus Pembrolizumab or Everolimus for advanced renal cell carcinoma. N Engl J Med. 2021;384(14):1289–300.
8. Rini BI, Plimack ER, Stus V, Gafanov R, Hawkins R, Nosov D, et al. Pembrolizumab plus Axitinib versus Sunitinib for advanced renal-cell carcinoma. N Engl J Med. 2019;380(12):1116–27.
9. Tucker MD, Rini BI. Predicting response to immunotherapy in metastatic renal cell carcinoma. Cancers (Basel). 2020;12(9):2662.
10. Gibellini L, De Biasi S, Porta C, Lo Tartaro D, Depenni R, Pellacani G, et al. Single-cell approaches to profile the response to immune checkpoint inhibitors. Front Immunol. 2020;11:490.
11. Hopkins AM, Rowland A, Kichenadasse G, Wiese MD, Gurney H, McKinnon RA, et al. Predicting response and toxicity to immune checkpoint inhibitors using routinely available blood and clinical markers. Br J Cancer. 2017;117(7):913–20.
12. Krishna C, DiNatale RG, Kuo F, Srivastava RM, Vuong L, Chowell D, et al. Single-cell sequencing links multiregional immune landscapes and tissue-resident T cells in ccRCC to tumor topology and therapy efficacy. Cancer Cell. 2021;39(5):662–677 e666. https://www.sciencedirect.com/science/article/pii/S1535610821001653?via%3Dihub
13. Cossarizza A, Chang HD, Radbruch A, Abrignani S, Addo R, Akdis M. Guidelines for the use of flow cytometry and cell sorting in immunological studies (third edition). Eur J Immunol. 2021;51(12):2708–3145.
14. Huang AC, Postow MA, Orlowski RJ, Mick R, Bengsch B, Manne S, et al. T-cell invigoration to tumour burden ratio associated with anti-PD-1 response. Nature. 2017;545(7652):60–5.
15. De Biasi S, Meschiari M, Gibellini L, Bellinazzi C, Borella R, Fidanza L, et al. Marked T cell activation, senescence, exhaustion and skewing towards TH17 in patients with COVID-19 pneumonia. Nat Commun. 2020;11(1):3434.
16. Roederer M, Nozzi JL, Nason MC. SPICE: exploration and analysis of post-cytometric complex multivariate datasets. Cytometry A. 2011;79(2):167–74.
17. Greene E, Finak G, D'Amico LA, Bhardwaj N, Church CD, Morishima C, et al. New interpretable machine-learning method for single-cell data reveals correlates of clinical response to cancer immunotherapy. Patterns, 2021;2(12):100372.

18. Nikolich-Zugich J. Ageing and life-long maintenance of T-cell subsets in the face of latent persistent infections. Nat Rev Immunol. 2008; 8(7):512–22.
19. Powell DJ Jr, Dudley ME, Robbins PF, Rosenberg SA. Transition of late-stage effector T cells to CD27+ CD28+ tumor-reactive effector memory T cells in humans after adoptive cell transfer therapy. Blood. 2005;105(1):241–50.
20. Kallies A, Good-Jacobson KL. Transcription factor T-bet orchestrates lineage development and function in the immune system. Trends Immunol. 2017;38(4):287–97.
21. Mahnke YD, Brodie TM, Sallusto F, Roederer M, Lugli E. The who's who of T-cell differentiation: human memory T-cell subsets. Eur J Immunol. 2013;43(11):2797–809.
22. Kluger HM, Tawbi HA, Ascierto ML, Bowden M, Callahan MK, Cha E, et al. Defining tumor resistance to PD-1 pathway blockade: recommendations from the first meeting of the SITC immunotherapy resistance taskforce. J Immunother Cancer. 2020;8(1):e000398.
23. Kawashima A, Kanazawa T, Kidani Y, Yoshida T, Hirata M, Nishida K, et al. Tumour grade significantly correlates with total dysfunction of tumour tissue-infiltrating lymphocytes in renal cell carcinoma. Sci Rep. 2020;10(1):6220.
24. Menard LC, Fischer P, Kakrecha B, Linsley PS, Wambre E, Liu MC, et al. Renal cell carcinoma (RCC) tumors display large expansion of double positive (DP) CD4+CD8+ T cells with expression of exhaustion markers. Front Immunol. 2018;9:2728.
25. Tripathi A, Lin E, Xie W, Flaifel A, Steinharter JA, Stern Gatof EN, et al. Prognostic significance and immune correlates of CD73 expression in renal cell carcinoma. J Immunother Cancer. 2020;8(2): e001467.
26. Teke K, Yaprak Bayrak B, Yuksekkaya M, Uslubas AK, Kosem ME, Yilmaz H, et al. Prognostic value of immunological profile based on CD8+ and FoxP3+ T lymphocytes in the peritumoral and intratumoral subsites for renal cell carcinoma. Int Urol Nephrol. 2020; 52(12):2289–99.
27. Bi K, He MX, Bakouny Z, Kanodia A, Napolitano S, Wu J, et al. Tumor and immune reprogramming during immunotherapy in advanced renal cell carcinoma. Cancer Cell. 2021;39(5):649–661 e645.
28. Zizzari IG, Napoletano C, Di Filippo A, Botticelli A, Gelibter A, Calabro F, et al. Exploratory pilot study of circulating biomarkers in metastatic renal cell carcinoma. Cancers (Basel). 2020;12(9):2620.
29. Julià EP, Mando P, Rizzo MM, Cueto GR, Tsou F, Luca R, et al. Peripheral changes in immune cell populations and soluble mediators after anti-PD-1 therapy in non-small cell lung cancer and renal cell carcinoma patients. Cancer Immunol Immunother. 2019;68(10): 1585–96.
30. Au L, Hatipoglu E, Robert de Massy M, Litchfield K, Beattie G, Rowan A, et al. Determinants of anti-PD-1 response and resistance in clear cell renal cell carcinoma. Cancer Cell. 2021;39(11):1497–1518.e11.

SUPPORTING INFORMATION

Additional supporting information may be found in the online version of the article at the publisher's website.

How to cite this article: De Biasi S, Guida A, Lo Tartaro D, Fanelli M, Depenni R, Dominici M, et al. Redistribution of CD8+ T cell subsets in metastatic renal cell carcinoma patients treated with anti-PD-1 therapy. Cytometry. 2022. https://doi.org/10.1002/cyto.a.24562